International Journal of Heat and Mass Transfer 91 (2015) 647–655

Contents lists available at ScienceDirect

International Journal of Heat and Mass Transfer

journal homepage: www.elsevier.com/locate/ijhmt

Constructal design of gas-cooled electric power generators, self-pumping and atmospheric circulation

A. Bejan [a,*], S. Lorente [b], J. Lee [c], Y. Kim [c]

[a] Duke University, Department of Mechanical Engineering and Materials Science, Durham, NC 27708-0300, USA
[b] Université de Toulouse, INSA, 135 Avenue de Rangueil, 31077 Toulouse, France
[c] Doosan Heavy Industries & Construction Co., Ltd., 22 Doosan Volvo-ro, Seongsan-gu, Changwon, Gyeongnam, South Korea

ARTICLE INFO

Article history:
Received 9 April 2015
Received in revised form 2 July 2015
Accepted 3 July 2015
Available online 22 August 2015

Keywords:
Constructal design
Cooling
Generators
Rotating electric machines
Self-pumping
Atmospheric circulation
Natural convection

ABSTRACT

Rotating electric machines generate heat volumetrically, and are cooled by forced convection aided by the self-pumping effect. In this paper we focus on the fundamental relationship between the internal flow architecture of the gas cooled winding and its thermal performance, which is represented by the nearly uniform distribution of peak temperature throughout the winding volume. We show that the cooling passages can be sized such that the volumetric cooling is most effective. From this finding follows the number of passages and their distribution through the heat generating volume. The principle is developed analytically, and it is then validated based on numerical simulations of the cooling architecture. The paper also reports the thermodynamics basis of the self-pumping effect, and its natural occurrence as free convection in general, which includes atmospheric circulation.

1. Introduction

In this paper we take a look from above at the improvements that can be made in the performance of cooling architecture of synchronous electric power generators for steam power plants. The focus is on fundamentals. The approach is based on constructal design [1,2] which is the philosophy that improvements in global performance are achievable through continuing changes in the geometry of the architecture of the flow system, to facilitate flow. For this purpose, the flow architecture must be free to morph, and the better and better flow architectures must be pursued relentlessly.

What designers view as "optimal" is the time direction in which the architectural changes are happening. The direction is natural, and is exhibited by the evolutionary designs of manmade systems (the evolution of technology) and, even more visibly, by the flow architectures of nature [2]. The natural evolutionary character of technology was illustrated recently by the evolution of aircraft [3].

Here we focus on the evolutionary design of gas-cooled synchronous generators powered by steam turbines in modern power plants [4–6]. The synchronous generator is a solid structure that generates heat volumetrically, and is cooled by a gas that flows through multi-scale channels embedded in the structure. The design of the structure (sizes, materials, shapes, connections) is the result of trade-offs between several key objectives: mechanical strength, stiffness, electromechanical power conversion, heat transfer (cooling) and fluid flow [7,8].

Traditionally these objectives were pursued separately, and the features that satisfied one objective served as constraints in the pursuit of features that satisfy the other objectives. More recently, computational design is making possible the search for features that satisfy several objectives simultaneously. Electric machines of all kinds are evolving toward compactness, which means higher power density. In this direction, the generation of heating per-unit volume increases, and so do the peak temperatures that threaten the mechanical integrity and electrical performance of the machine. Effective volumetric cooling is of paramount importance in the future of electric machines.

In this paper we address the fundamentals of the volumetric cooling of the machine structure. The approach is based on constructal design, which is the view that the heat and fluid flow structure morphs freely as we search for a higher heat transfer density, lower peak temperatures, and a more uniform distribution of the allowable temperature level throughout the machine volume. Key are the continuous changes in the geometry of the solid, in the direction of greater compactness.

* Corresponding author.
E-mail address: abejan@duke.edu (A. Bejan).

http://dx.doi.org/10.1016/j.ijheatmasstransfer.2015.07.015
0017-9310/

Nomenclature

c_P	specific heat, J kg^{-1} K^{-1}
d_a	length, m
D	diameter, m
H	height, m
k	thermal conductivity, W m^{-1} K^{-1}
L	length, m
L_r	rotor length, m
L_t	spacing between bars, m
L_c	core length, m
$\dot{m}$	mass flow rate, kg s^{-1}
n	number of core packages
q, $\dot{Q}$	heat current, W
$\tilde{q}$	dimensionless heat current, Eq. (24)
r	outer radius of bars, m
R	radius, m
Re_H	Reynolds number, Eq. (5)
S	spacing, m
T	temperature, K
T_{max}	peak temperature, K
T_0	inlet temperature, K
V	fluid velocity, m s^{-1}
W	width, m
$\dot{W}$	pumping power, W

Greek letters

δ	boundary layer thickness, m
ΔP	pressure drop, Pa
μ	viscosity, kg s^{-1} m^{-1}
ν	kinematic viscosity, m^2 s^{-1}

Subscripts

b	bar
c	core
out	outlet
r	radial
r	rotor
x	axial

2. Configuration

The cooling gas enters the volume of the generator as a single stream. The channels distribute this stream throughout the volume such that the coolant bathes the smallest features of the heat generating structure. Finally, the warmed up coolant is reconstituted as a single stream and is led to an external system to be cooled before being reused (Fig. 1).

Heat is generated non-uniformly in three dimensions. The stator structure generates and conducts heat longitudinally along the bars and radially along the laminations. The stator structure is hierarchical: laminations are stacked into packages that are swept by coolant, and packages are grouped into sections that are permeated by coolant that flows in a particular radial direction, toward the axis, or away from the axis. Heat is also convected radially along the cooling channels. The key feature to be discovered is the channel spacing, or the number of packages in one section (Fig. 2).

In current designs, the rotor winding has the highest heat generation density. Its heat and fluid flow structure (Figs. 3 and 4) is similar to the stator structure. Heat is generated and conducted longitudinally in the electrical conductors of the magnetic field winding. Heat is intercepted by the coolant and convected radially through radial spacings. The flow of coolant through the rotor is always outward, toward the relative motion gap between rotor and stator.

In summary, the flow of heat is in steady-state, from the cylindrical volume of the machine to the stream of coolant that flows through the volume. The coolant flows through multiple channels: it is distributed non uniformly and hierarchically though few large and many small channels. A fan drives the flow of coolant. In the rotor, the flow is augmented (aided) by the self-pumping effect that emerges when the coolant is heated by the solid structure. Self-pumping is another name for natural convection (or chimney flow) through radial channels. The pressure difference generated by this effect is given in Section 4.

The cross sectional shapes of the rotor and stator volumes with heat generation and radial flow are annular. In each annulus, the radial thickness is not much larger than the inner radius. Consequently, the annular space can be modeled as a two-dimensional space, as shown in Fig. 5. The radial dimension of this space (H) is the radial length traveled by the coolant. The axial dimension of this space (L) is the distance between two consecutive cooling channels. The channel spacing (S) and the solid thickness (L) may vary.

In the rotor (r) and the stator (s) the conduction through the spaces filled with solid (the windings) is anisotropic. In the rotor, the axial thermal conductivity (k_{rx}) is greater than the radial conductivity (k_{rr}). In the laminations of the stator, the opposite is true: the radial conductivity (k_{sr}) is greater than the axial conductivity (k_{sx}).

The anisotropy of the stator is complicated further by the thermal conductivity of the stator bars (k_{bx}), which is greater than k_{sr} and k_{sx}. The fluid flow through the stator is also complicated by the fact that the channel flows may be oriented in counterflow, unlike the parallel flows through the rotor winding.

3. Parallel flow

Consider one of the heat generating volumes (in the rotor, or the stator, Fig. 6), and treat it as a two-dimensional volume of longitudinal length L_r (the rotor length), transversal flow length H, and third dimension πD, where D is the diameter of the relative motion gap. The total heat generation rate removed from this volume is q. The total mass flow rate of fluid that bathes this volume is $\dot{m}$.

There are n radial slits of flow length H and spacing S, where $n = L_r/L$, and L is the axial dimension of each heat generating section k_x, cf. Fig. 6. The coolant is an ideal gas. It enters the slit at the temperature T_0, and exits at the temperature T_{out}, which is to be determined. The maximum allowable temperature (T_{max}) occurs at hot spots located in the exit plane, midway between two consecutive exits. The objective is to configure the flow such that ($T_{max} - T_0$) and the fan (pump) power are small when q and $\dot{m}$ are specified. In the limit of small S and large n, the flow through the volume resembles Poiseuille flow through parallel-plates channels (Fig. 7, left). In this limit, T_{out} approaches T_{max}, and the entire plane with the outlets is isothermal, at T_{max}. The coolant ($\dot{m}$) enters the volume at T_0, and exits at T_{max}, therefore $q = \dot{m}c_P(T_{max} - T_0)$. The performance is indicated by the ratio

$$\frac{T_{max} - T_0}{q} = \frac{1}{\dot{m}c_P} \tag{1}$$

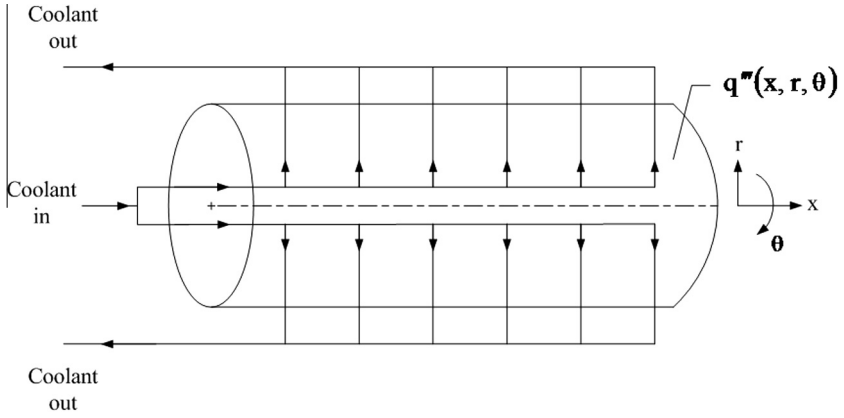

Fig. 1. Coolant flow paths through the rotor and stator of a generator.

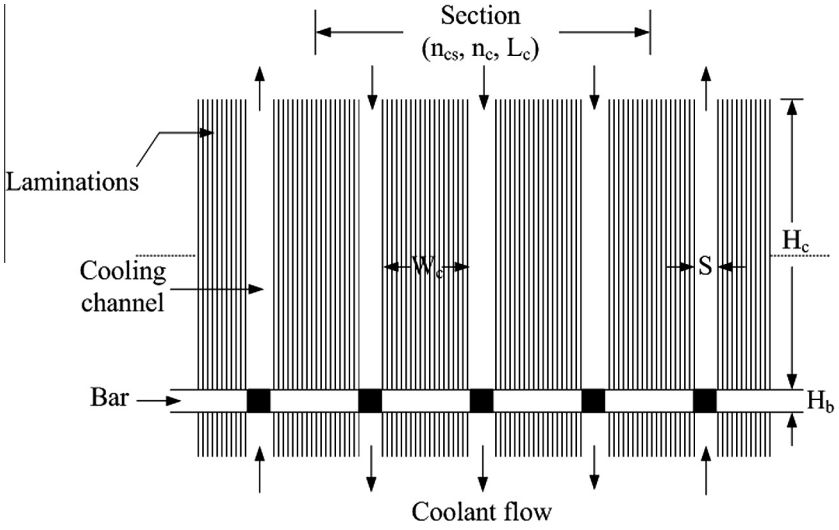

Fig. 2. The laminated structure of the stator, showing the cooling channels, the stator bar, and one section through which the coolant flows in one direction.

This comes at a cost in pressure drop, because ΔP in Poiseuille flow increases fast as S decreases Ref. [1, p. 113],

$$\Delta P \sim \frac{\dot{m}}{n}\nu\frac{H}{S^4} \tag{2}$$

In the opposite limit, the spacings S are large enough so that the fluid temperature is T_0 throughout the channel volume (Fig. 7, middle). In addition, assume that the flow along each channel (with small ΔP, because S is large) is fast enough so that the surfaces of the channel are essentially at T_0. This means that the removal of the heat generation rate is limited by solid conduction in the axial direction (perpendicular to the channel), where k_x stands for either k_{rx} or k_{sx},

$$q \sim 2nk_x\pi DH\frac{T_{max}-T_0}{L/2} \tag{3}$$

which yields

$$\frac{T_{max}-T_0}{q} \sim \frac{L^2}{4\pi k_x HDL_r} \tag{4}$$

The third design to consider is in-between. It is the design with constructal spacings (Ref. [1, Ch. 3]), in which $S \sim 2\delta$, and δ is the thickness of the laminar boundary layer that lines every surface of flow length H (Fig. 7, right). If the flow is laminar, then, in an order of magnitude sense,

$$\delta \sim 3HRe_H^{-1/2} \tag{5}$$

where $Re_H = VH/\nu$. The factor 3 appearing in Eq. (5) is an approximation of the factors appearing in the Blasius solution (factor 4.92) and the displacement-thickness solution (factor 1.73) [9]. The mean fluid velocity along the channel is

$$V = \frac{\dot{m}/n}{\rho S\pi D} \tag{6}$$

The spacing is therefore

$$\frac{S}{H} \sim 10^2\mu\frac{DL_r}{\dot{m}L} \tag{7}$$

The solid thickness L is determined as follows. The total heat transfer rate is expressed in two ways,

$$q = \dot{m}c_P(T_{out}-T_0) \tag{8}$$

$$q = 2nH\pi Dk_x\frac{T_{max}-T_{out}}{L/2} \tag{9}$$

where we assumed that the channel surface is at T_{out}. Combining Eqs. (8) and (9) we obtain

$$\frac{T_{out}-T_0}{T_{max}-T_{out}} \sim \frac{4\pi k_x HDL_r}{\dot{m}c_P L^2} \tag{10}$$

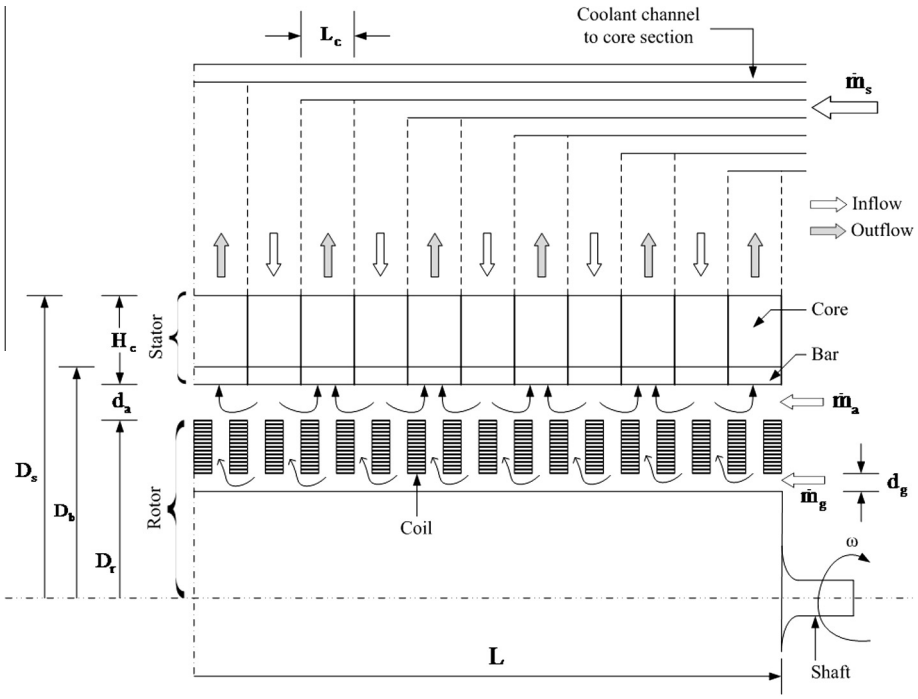

Fig. 3. Detail of the dimensions of the flow architecture, and the continuity of coolant flow between the rotor coils and the stator core.

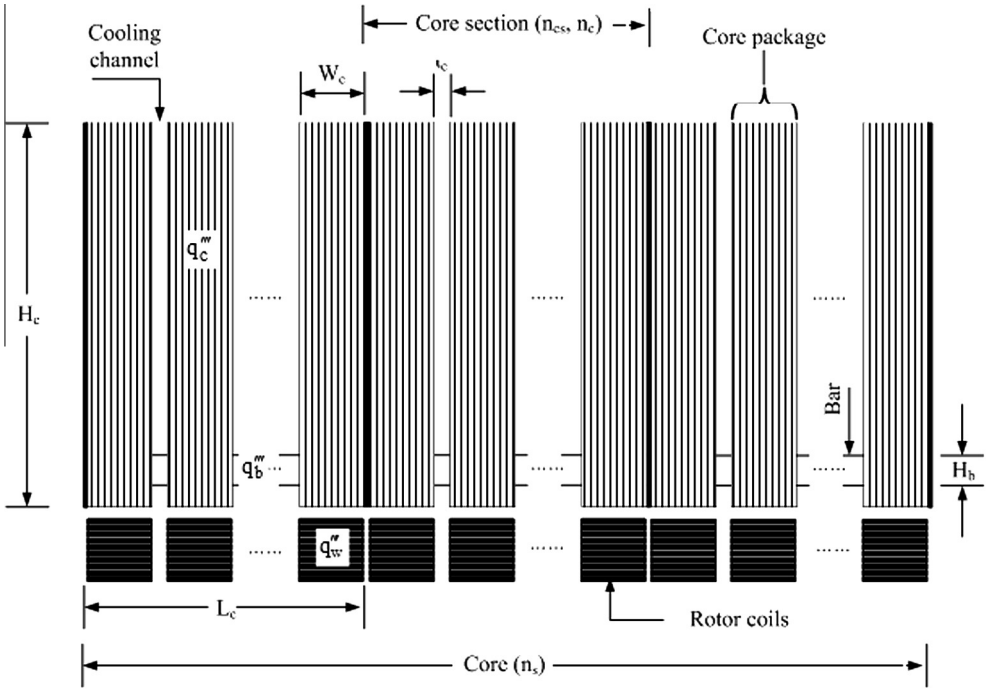

Fig. 4. Details of the dimensions of the stator structure.

Next, the continuity of heat flux at the fluid–solid interface requires

$$k\frac{T_{out}-T_0}{S/2}\sim k_x\frac{T_{max}-T_{out}}{L/2} \tag{11}$$

which yields

$$\frac{T_{out}-T_0}{T_{max}-T_{out}}\sim\frac{k_xS}{kL} \tag{12}$$

Note that in Eq. (11) we wrote k for the fluid thermal conductivity, and because the fluid has a Prandtl number close to 1, the thermal boundary layer thickness is the same as the velocity boundary layer thickness, $\delta\sim S/2$. Combining Eqs. (10) and (12) we arrive at

$$SL\sim 4\pi\frac{kHDL_r}{c_P\dot{m}} \tag{13}$$

which agrees with Eq. (7) because the Prandtl number $\nu/\alpha(=\mu c_P/k)$ is a constant of order 1. Note that S increases when L decreases, and vice versa.

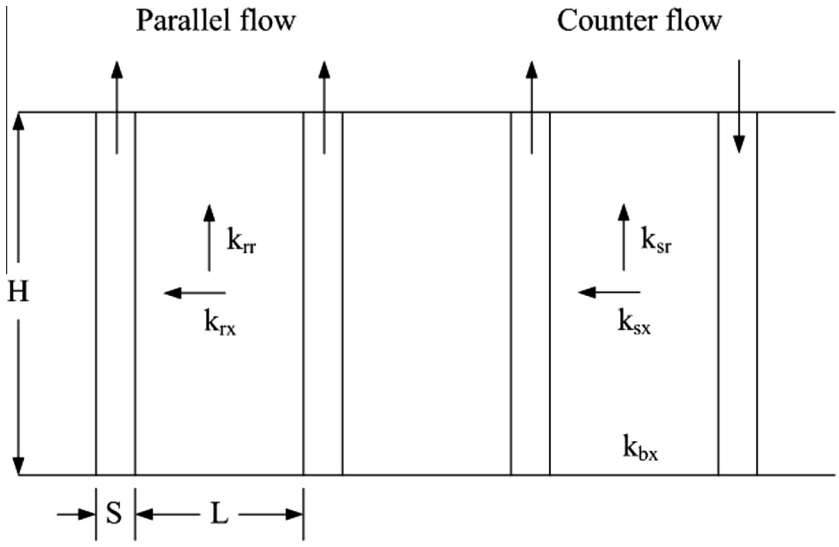

Fig. 5. Parallel flow versus counter flow through a two dimensional conducting body with internal heat generation.

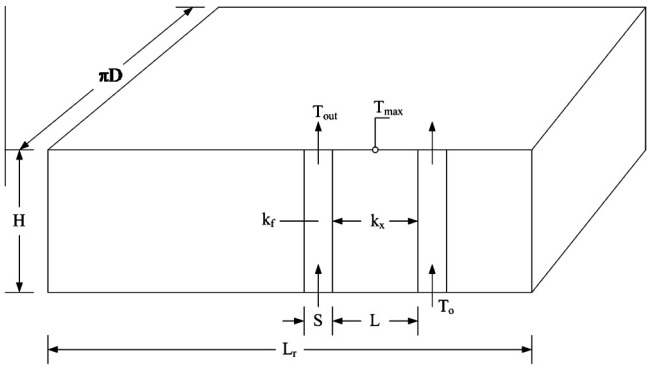

Fig. 6. Parallel flow model of a gas-cooled stator structure.

The figure of merit $(T_{max} - T_0)/q$ is obtained by eliminating T_{out} between Eqs. (8) and (9),

$$\frac{T_{max} - T_0}{q} \sim \frac{1}{\dot{m}c_P} + \frac{L^2}{4\pi HDk_xL_r} \tag{14}$$

This shows that the lowest level of peak temperatures corresponds to the small-S limit represented by Eqs. (1) and (2). Small packages (L) approach the limit of Eqs. (1) and (2).

4. Self pumping

The pressure drop for this design continues to be given by Eq. (2), which is the same as writing

$$\Delta P \sim \frac{\dot{m}\nu HL}{L_rS^4} \tag{15}$$

Because SL varies as $1/\dot{m}$, cf. Eq. (13), we conclude that $L \sim 1/(\dot{m}S)$ and consequently the pressure drop varies as S^{-5}. The pumping power that is required to overcome ΔP has the order of magnitude

$$\dot{W} = \frac{\dot{m}\Delta P}{\rho} \sim \frac{\dot{m}^2\nu HL}{\rho L_rS^4} \tag{16}$$

In the rotor, the self-pumping effect reduces the ΔP by a fraction that can be estimated as follows. As shown in Fig. 8, the cold coolant enters along the rotor axis at the temperature T_0. The coolant is then accelerated to the rotor radius R (the relative motion gap), where its pressure and temperature increase to P_R and T_R. We assume that the rotor radius is considerably smaller than the rotor length, such that most of the heating experienced by the $\dot{m}$ stream occurs at high pressure, at the rotor radius, in the windings. According to the same model, the flow of $\dot{m}$ in the radial direction is approximated as reversible and adiabatic:

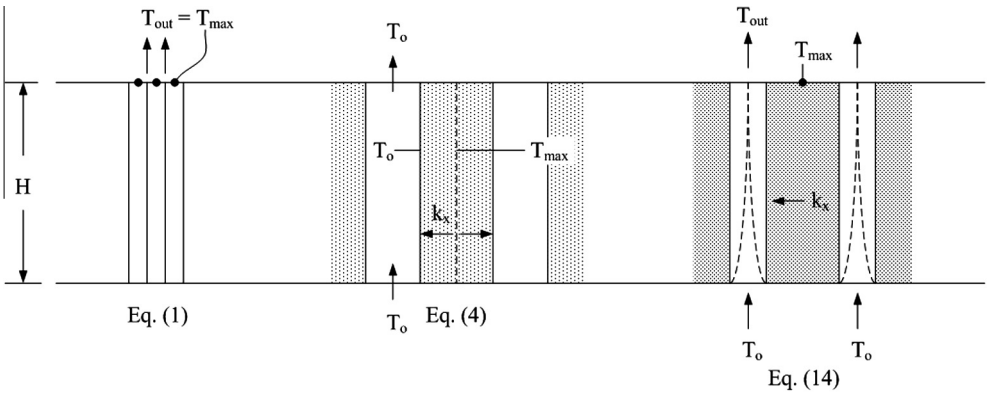

Fig. 7. The two extremes of the flow structure of Fig. 5: from small spacings, Eq. (1), to large spacings, Eq. (14).

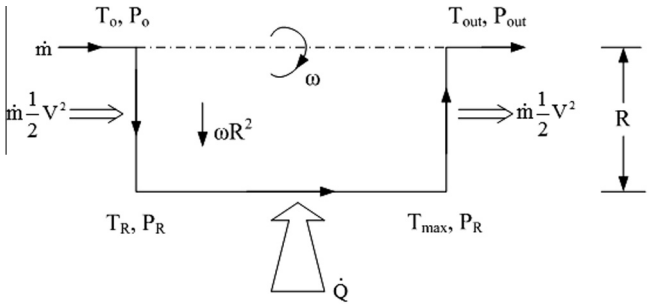

Fig. 8. The origin of the self pumping effect experienced by a stream that is accelerated to a larger radius of rotation, and then heated at that radius.

$$\frac{T_R}{T_0} = \left(\frac{P_R}{P_0}\right)^{R/c_P} \tag{17}$$

The work that the $\dot{m}$ stream of coolant receives from the radial passages, en route from the axis to the outer radius is

$$\dot{W} = \dot{m}\frac{1}{2}V^2 \tag{18}$$

where $V = \omega R$ is the peripheral velocity with angular speed ω[rad/s]. This work input is fixed, and matches the specific enthalpy rise as the stream flows adiabatically from axis to rotor periphery,

$$\frac{1}{2}V^2 = c_P(T_R - T_0) \tag{19}$$

While flowing longitudinally (at constant pressure, P_R) and cooling the rotor winding, the $\dot{m}$ stream receives the heat input $\dot{Q}$, and its temperature rises from T_R to T_{max},

$$\dot{Q} = \dot{m}c_P(T_{max} - T_R) \tag{20}$$

Next, the coolant flows from the outer radius to the rotor axis, and it expands isentropically from P_R to the final pressure P_{out},

$$\frac{T_{max}}{T_{out}} = \left(\frac{P_R}{P_{out}}\right)^{R/c_P} \tag{21}$$

while delivering back to the radial passages the power $\dot{m}\frac{1}{2}V^2$, cf. Eq. (19). Alternatively, the first law analysis of the control volume that contains the entire U-shaped flow path of Fig. 8, shows that $\dot{Q}$ is also equal to

$$\dot{Q} = \dot{m}c_P(T_{out} - T_0) \tag{22}$$

By combining Eqs. (17) and (20)–(22), we arrive at the self-pumping effect represented by the pressure rise along the axis,

$$\frac{P_{out}}{P_0} = \frac{P_R}{P_0}\left(\frac{\tilde{q}+1}{\tilde{q}+T_R/T_0}\right)^{c_P/R} \tag{23}$$

where

$$\tilde{q} = \frac{\dot{Q}}{\dot{m}c_P T_0} \tag{24}$$

Noteworthy is that the radial temperature ratio T_R/T_0 is set by the power indicated in Eqs. (18) and (19). As a consequence of Eq. (17), the radial pressure ratio P_R/P_0 is fixed as well.

Eq. (23) shows that the self-pumping effect P_{out}/P_0 depends on the heating (q) that the coolant receives from the winding. When the heating is sufficiently large such that $\tilde{q} > T_R/T_0$, the axial pressure rise reaches its highest value,

$$\frac{P_{out}}{P_0} \to \frac{P_R}{P_0} = \left(\frac{T_R}{T_0}\right)^{c_P/R} = \left(1 + \frac{V^2}{2c_P T_0}\right)^{c_P/R} \tag{25}$$

When the heating effect is negligible ($\tilde{q} < 1$), the self-pumping effect indicated by Eq. (23) is negligible,

$$\frac{P_{out}}{P_0} \sim 1 \tag{26}$$

We return in Section 6 to the self-pumping effect and its occurrence in nature.

5. Number of core packages

In this section, we report the results of numerical simulations of the heat transfer in the rotor, and the effect of the number of core packages. As a first step, we select the domain in which to model numerically the very complicated architecture of the generator. The problem is three-dimensional because of the presence of the longitudinal bars. Key is the search for symmetry planes that will allow to simplify as much as possible the numerical simulations. Longitudinally, we have a sequence of core packages (thickness W_c) and gas spacing (thickness S), as shown in Fig. 2. This sequence leads to the existence of the two first planes of symmetry that we will use in the modeling. The longitudinal dimension of the control volume is $(W_c + S)/2$.

The height of the domain is set by the height of the core packages, H_c. The focus must be on the stator part of the generator. Therefore we add to H_c the distance between the outer radius of the rotor and the inner radius of the stator, d_a (Fig. 3). H_c and d_a are fixed. We also add to the height of the computational domain a distance located at the outer radius of the stator.

We repeat the procedure in the transversal direction with the objective to discover the planes of symmetry where they exist. The stator bar is made of 42 elemental bars positioned radially and separated by a constant angle (Fig. 9). The outer radius of the bars is named r, while W_b is the transversal thickness of each bar. The gas gap between two bars is called L_t, and is calculated as $2\pi r = 42(W_b + L_t)$. The combination of gas gap and bar leads to two new planes of symmetry, one in the bar, and the other one in the gas gap. The thickness of the control volume in the transversal direction is therefore $(W_b + L_t)/2$.

In summary, the control volume (Fig. 9) is modeled as a parallelepiped with the dimensions:

- Height: $d_a + H_c + d$
- Longitudinal thickness: $(W_c + S)/2$
- Transversal thickness: $(W_b + L_t)/2$, where L_t is the spacing between bars.

As an example for the numerical simulations, we choose $d_a = 10$ cm, $H_c = 70$ cm, $d = 10$ cm, $W_b = 2.5$ cm, $L_t = 8$ cm. The total volume of material is fixed, together with the size of the generator. Furthermore, the core height is also fixed, because of mechanical and electrical constraints. The degree of freedom will be the longitudinal thickness, and its components W_c and S. In other words, we study the allocation of the combination of material & fluid so that the maximum temperature reached by the material remains below T_{max}.

Fig. 10 shows the control volume, the stator tooth, the stator bar and the stator yoke. The final version of the control volume with the four domains to model can be seen in the fifth drawing of Fig. 10. The remaining volume (the difference between the control volume and the four solid parts) is occupied by the flowing fluid.

The configuration is one of heat transfer and fluid flow, with conduction heat transfer in the solid. We model heat conduction inside the different types of solids and forced convection in the fluid. The fluid is hydrogen, and the flow is turbulent. We chose the k–ε turbulence model, and solved the conservation of mass,

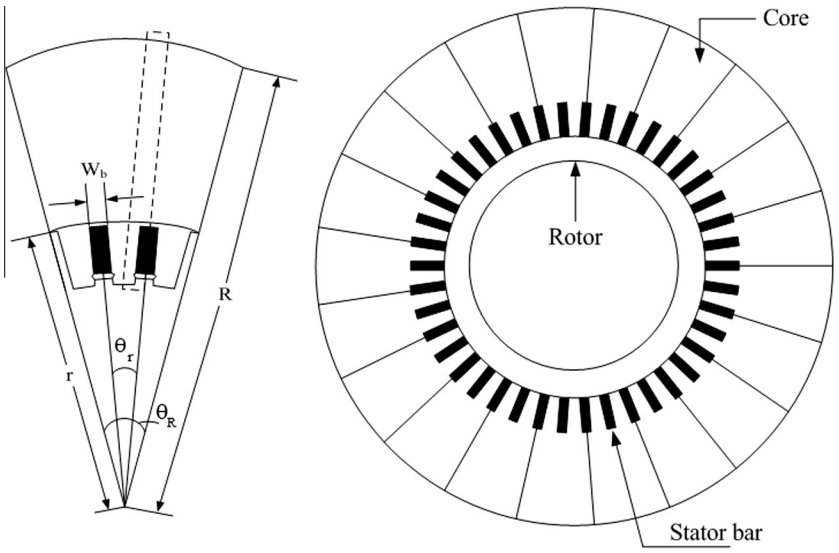

Fig. 9. Cross section through the rotor and the stator. The detail shows the computational domain.

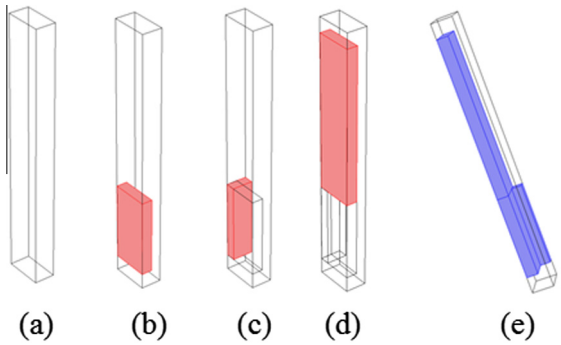

Fig. 10. The subdomains of the elemental volume, from left to right: the computational domain, the stator core, the stator bar, the stator core yoke, and the subdomains together.

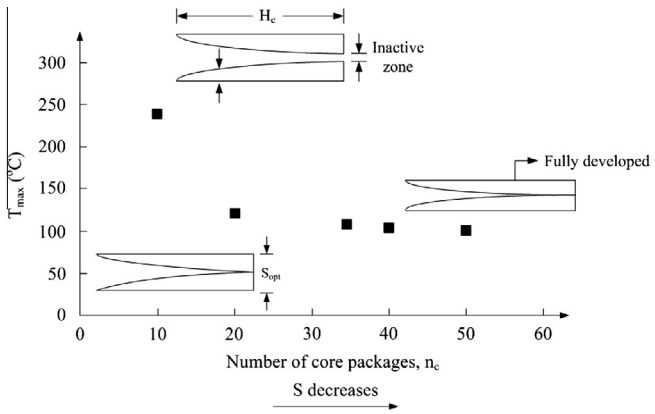

Fig. 11. The effect of complexity: the peak temperature versus the number of core packages.

momentum and energy in the fluid, together with conservation of energy in the solid parts. The numerical problem was solved using a finite element package [10]. The computations were performed first with a coarse mesh, then with finer meshes. When the maximum temperature change become of about 2 percent it was considered that the solution was mesh independent.

The boundary conditions are specified on four planes of symmetry in the transversal direction, one inlet in the longitudinal direction at the exit from the rotor, and one longitudinal outlet at the exit from the stator. The inlet temperature is moderate.

In addition, we attributed a volumetric heat density to each solid part: core tooth, core yoke and bar. The core yoke and tooth are made of SiO_2. We applied a non-isotropic thermal conductivity by stating that the transversal thermal conductivity is five times larger than the conductivities in the other two directions. The bar is made of copper.

The coolant is hydrogen. Even though helium is inert and non-flammable, it cannot be obtained sufficiently in quantities, which makes its price high and makes it unsuitable as cooling medium. Hydrogen can be obtained rather inexpensively, and it has advantages over helium in having a small density and better thermal characteristics. These factors combine to make hydrogen an ideal coolant, but there is one major flaw that it is explosive when mixed with air and exposed to an ignition source. However, if the purity of the hydrogen gas can be maintained at a very high level, then, an explosion does not occur even if an ignition source is present. The hydrogen mass flow rate provided by the rotor rotation is fixed, and so is the inlet velocity. The inlet velocity is 2 m/s, corresponding to about 40 m/s near the bar. Assume that the total rotor length is L (fixed), and the core length is L_{c1}. If we have n_{c1} cores, then $n_{c1} \times L_{c1} = L$. If one core is made of n_1 channels, then $L_{c1} = n_1 \times (W_{c1} + S_1)$. The total mass flow rate is $n_{c1} \times n_1 \times \dot{m}_1$ with $\dot{m}_1$ as a function of $V_{inlet,1} \times (W_{c1} + S_1)$.

If we have n_{c2} cores, then $n_{c2} \times L_{c2} = L$. If one core is made of n_2 channels, then $L_{c2} = n_2 \times (W_{c2} + S_2)$. The total mass flow rate is $n_{c2} \times n_2 \times \dot{m}_2$, with $\dot{m}_2$ as a function of $V_{inlet,2} \times (W_{c2} + S_2)$. Because $L = n_{c1} \times n_1 \times (W_{c1} + S_1) = n_{c2} \times n_2 \times (W_{c2} + S_2)$, we conclude that $V_{inlet,1} = V_{inlet,2}$. We fixed the number of core packages, calculated the corresponding thickness and the spacing value, and simulated the model numerically. For each simulation we extracted from the results the maximum temperature. We found that the maximum temperature is always located in the vicinity of the bar, as one would expect.

Fig. 11 shows the maximum temperature as a function of the number of core packages. If the maximum admissible temperature is known, then the designer can select the number of core packages and the corresponding gap between them such that the solid reaches the maximum temperature value.

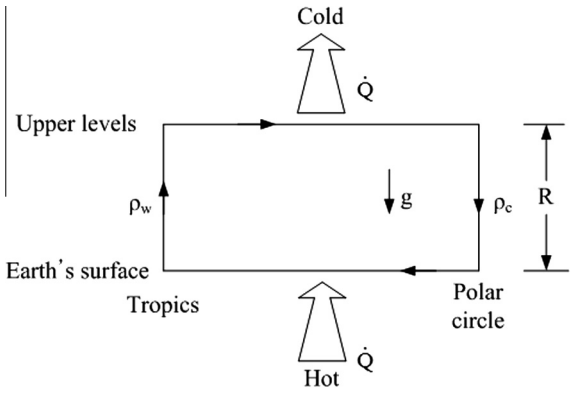

Fig. 12. The natural circulation of the atmosphere in the plane of the meridian is driven as a heat engine, which is equivalent to the self-pumping effect discussed in Fig. 8.

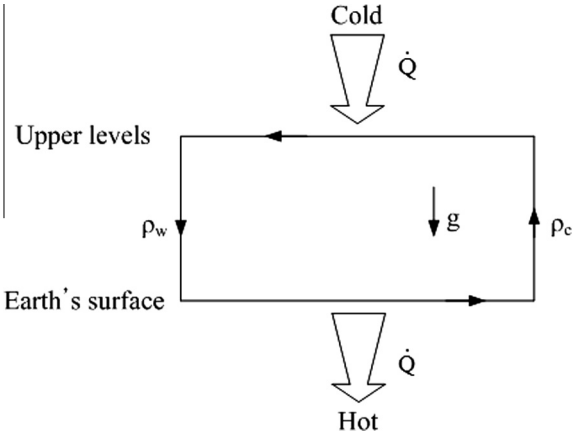

Fig. 13. The reverse of the circulation sown in Fig. 12 is impossible, because by itself the heat current $\dot{Q}$ does not flow from cold to hot.

Fig. 11 also shows that increasing the number of core packages has the effect of decreasing the maximum temperature. Interesting is that most of the decreases in T_{max} occurs as n_c increases to approximately 20, above which the decrease in T_{max} is marginal as n_c increases to 50. Because the simpler design is preferable, $n_c \sim 20$ is an important feature to seek for the design of stator cooling. This conclusion confirms the existence of an optimal spacing, cf. Fig. 7 and Eq. (14). The Reynolds number based on the swept length ($H_c \sim 30$ cm) and mean fluid velocity (30 m/s) is of order 1.5×10^5. The boundary layer thickness is of order 0.25 cm, therefore the optimal spacing is of order 0.5 cm. This is in agreement with the spacing S that corresponds to $n_c \sim 20$ in Fig. 11, because $S_t \sim 10$ cm is the total cooling spacing, therefore $S \sim S_t/n_c = 10\text{ cm}/20 = 0.5$ cm.

6. Conclusions, and atmospheric circulation

The main conclusion is that the path to increasing the cooling performance of the rotating electrical machine is by allowing the geometric features of the flow architecture to vary freely, on the way to decreasing the temperature peaks, wherever they may occur. This approach is in accord with the evolutionary direction sketched in Section 1.

For example, we showed that the allocation of the gas volume has a profound effect on decreasing the peak temperatures, cf. Fig. 11. Important is the conclusion that the act of increasing the number of core packages reaches diminishing returns. There is a critical number ($n_c \simeq 20$) above which further increases in n_c and flow architecture complexity do not yield significant decreases in the peak temperature.

On a more fundamental level, the thermodynamics basis of the self-pumping effect (Section 4) sheds light on all the phenomena of natural circulation that occur at all scales in nature. The earth-size equivalent of the flow of Fig. 8 is shown in Fig. 12, which represents the circulation of the atmosphere in the plane of the meridian. The atmospheric layer has the finite depth h, which is much smaller than the meridian length scale. Near the tropics, the air is warm (average density ρ_w) and the bottom-top hydrostatic pressure difference is of order $\Delta P_w \sim \rho_w g h$. Near the polar circle, the air is colder (average density ρ_c) and the bottom top hydrostatic pressure difference is of order $\Delta P_c \sim \rho_c g h$.

Note that $\Delta P_c > \Delta P_w$, because $\rho_c > \rho_w$. Furthermore, because the pressure at the upper surface of the atmosphere is uniform (zero), ΔP_w and ΔP_c represent the pressure exerted by the atmosphere on the ground. It follows that from the polar circle to the tropics, the pressure drop at ground level is of order $\Delta P = \Delta P_c - \Delta P_w \sim (\rho_c - \rho_w)\, g\, h$. This pressure difference drives the entire circulation, against friction. The pressure difference is due to the fact that at ground level (i.e., at high pressure) the cold air that descended from the upper levels is heated by the solar heat current $\dot{Q}$, absorbed originally by the earth's surface. As the circulation is completed at the upper levels, flowing from the tropical regions to the polar regions, the air current is cooled by radiation to the cold sky.

In sum, the circulation of air in Fig. 12 is the same as the circulation of the working fluid in a Rankine cycle or Brayton cycle, in this sequence: heating at high pressure is followed by cooling at low pressure. This is analogous to the sequence of processes identified in Fig. 8, although in that figure the cooling of $\dot{m}$ at low pressure (in the stationary frame of the laboratory) is not shown. The self-pumping effect that occurs in gas-cooled rotating windings is the same physics as all the natural circulation phenomena recognized broadly as natural convection, free convection, and buoyancy driven flow. The g of Fig. 12 plays the same role as the $\omega^2 R$ of Fig. 8.

Equally important is the observation that the circulation explained in Figs. 8 and 12 cannot proceed in the opposite sense. Cooling at high pressure (at ground level) cannot happen after (or before) heating at low pressure (at upper levels). The reverse flow sketched in Fig. 13 is impossible because, by itself, the heat current $\dot{Q}$ does not flow from the cold sky to the warm surface of the earth. Note also that the circulation imagined in Fig. 13 is the same as the circuit executed by the working fluid in a vapor compression or Brayton refrigeration cycle. In order to run (to force a heat current from cold to hot), a refrigerator requires an external power input. There is no external power that could drive the heat flow shown in Fig. 13.

In conclusion, self-pumping and heat-engine circulation (Figs. 8 and 11) occur naturally, as part of physics. The "refrigerator" circulation (Fig. 13) is impossible.

Conflict of interest

None declared.

References

[1] A. Bejan, S. Lorente, Design with Constructal Theory, Wiley, Hoboken, 2008.
[2] A. Bejan, S. Lorente, Constructal law of design and evolution: physics, biology, technology, and society, J. Appl. Phys. 113 (2013) 151301.
[3] A. Bejan, J.D. Charles, S. Lorente, The evolution of airplanes, J. Appl. Phys. 116 (2014) 044901.

[4] M. Tari, K. Yoshida, S. Sekito, R. Brütsch, J. Allison, A. Lutz, HTC insulation technology drives rapid progress of indirect-cooled turbo generator unit capacity, Power Engineering Society Summer Meeting (IEEE), 15–19 July 2001, Vancouver, pp. 1427–1432.
[5] M. Fujita, Y. Kabata, T. Tokumasu, M. Kakiuchi, H. Shiomi, S. Nagano, Air-cooled large turbine generator with multiple-pinched ventilation ducts, Electrical Machines and Drives, IEEE International Conference, 15 May 2015, San Antonio, TX, pp. 910–917.
[6] K. Hattori, K. Ide, K. Kobashi, T. Watanabe, Air-cooled large turbine generator with inner cooler ventilation system, CIGRE, 2002, Paris, Session 2002, 11-104.
[7] A.E. Fitzgerald, C. Kingsley, S.D. Umans, Electric Machinery, McGraw-Hill, New York, 1990.
[8] S. Timoshenko, S. Woinowsky-Krieger, Theory of Plates and Shells, McGraw-Hill, New York, 1959.
[9] A. Bejan, Convection Heat Transfer, fourth ed., Wiley, Hoboken, 2013.
[10] <www.comsol.com>.